NASA-CR-193288

SECA-FR-93-10

RADIATION/CONVECTION COUPLING IN ROCKET MOTOR & PLUME ANALYSIS

Contract No. NAS8-39811
Final Report

Prepared by:

A.J. Saladino
R.C. Farmer

Prepared for:

National Aeronautics & Space Administration
George C. Marshall Space Flight Center
Marshall Space Flight Center, AL 35812

SECA, Inc.
Suite 202
3313 Bob Wallace Avenue
Huntsville, AL 35805

July, 1993

PROJECT SUMMARY

Radiation heat transfer in rocket motor combustion chambers and plumes has historically been analyzed by simulating the flowfield without considering radiation, and as a second step calculating the radiation without modifying the flowfield solution. New and advanced propulsion system concepts have made these thermal fields more severe, so that the uncoupled solutions are no longer acceptable. This study coupled the radiative transport directly to the conservation equations and, thereby, yielded a simultaneous solution to all of the governing equations.

The three commonly used propellant systems: H_2/O_2, RP-1/O_2, and solid propellants radiate as: molecular emitters, non-scattering small particles, and scattering larger particles, respectively. This study addressed all of these types of radiation. Methods of representing the spectral character of these radiators were reviewed to select the most efficient radiation models for use in a coupled solution. Line-of-sight (LOS) calculations were made to verify that the radiation models selected were sufficiently accurate for radiation heat transfer predictions.

The nature of the radiation/convection coupled problem is that the divergence of the radiative heat flux must be included in the energy equation and that the local, volume averaged intensity must be determined by a solution to the radiative transfer equation (RTE). For a rigorous solution, the RTE must be solved along several LOS at each point in the flowfield at each computation step. Such a procedure is extremely costly; therefore, approximations are needed. The ordinary and improved differential approximations were developed to provide the required solution. Both of these solutions were provided as additions to the FDNS code (a Navier-Stokes solver for turbulent, two-phase combusting flow) to form the radiation/convection coupled solution. The ordinary differential approximation is applicable to combustion chambers where the flowfield is optically dense, and the improved differential approximation is applicable to nozzle flow and plumes which are of intermediate optical depth.

The thermal analysis provided by this radiation/convection coupled methodology is applicable to rocket motor and vehicle base heating design. It is of particular value in analyzing ablator material response in solid rocket motors and in gas/solid combustion phenomena in hybrid rocket motors, where the radiation heat load is critical to the system performance. Industrial applications to coal-fired furnace and glass melting-pot analyses are also feasible.

Table of Contents

RADIATION/CONVECTION COUPLING IN ROCKET MOTOR & PLUME ANALYSIS

1.0 Introduction

A computational fluid dynamics (CFD) code is presented which fully couples the radiation/convection interaction. Radiation heat flux is included in the energy equation, and the radiation transport equation is solved. These radiative terms and equations were added to the FDNS CFD code. Justification for choosing the radiation methods presented herein are given, along with the limitations of these methods, for various motor types. The code is flexible in that higher order radiative approximations can be added to the current order, as needed.

1.1 Methodology

Radiation within a flowfield depends upon the absorption and emission of electromagnetic energy to or from gaseous and particulate species. In the case of particles, there is an additional effect caused by the scattering of photons toward or away from a point, from all locations and directions within the flowfield. To account for these effects, the first step was to determine the radiative properties of the constituent species, namely the absorption and scattering cross-sections. The next step required the solution to an approximation to the integro-differential radiative transport equation (RTE). This resulted in two approximate methods, one valid for optically thick regions and the other valid for arbitrary optical thicknesses. Finally, the radiative source term is determined and added to the right-hand-side of the energy equation, providing the coupling between the radiation and CFD solvers.

2.0 Absorption and Scattering Coefficients

The three types of rocket motors currently being used - H_2/O_2, RP-$1/O_2$, and solid motors - radiate in the following manner:

1. Molecular radiation - infrared, non-luminous gaseous radiation associated mainly with rotational and vibrational energy modes; important for SSME nozzles with H_2O products.

2. Non-scattering small particles, comprised mostly of soot, and applicable to RP-$1/O_2$ engines. The molecular radiators: CO_2 and H_2O are also important in these engines.

3. Scattering large particles; specifically, those associated with solid propellants with Al_2O_3 products. Again, molecular radiators are also important.

This project addressed the radiation associated with H_2O, CO_2 and Al_2O_3. Absorption and emission by soot will be added at a later date.

2.1 Molecular Radiation

Two methods were coded for the gaseous radiators - the total emissivity or mean band model and the wide band model. The former method assumes that the spectral width of each band is narrow, allowing an essentially constant Planck function over the range of each band so that all the bands are integrated to evaluate a total emissivity. Although band overlap is considered negligible, provisions are made to correct for this effect. However, since the emissivity is

obtained as an average over all bands, this method was not used for the gas radiation properties. The wide band model is a more rigorous procedure for finding absorption coefficients, and it also provides these absorption coefficients as a function of wavelength. This is an important requirement since the partial differential equation approximation obtained from the RTE is solved for a single wavelength. In the wide band model the entire spectral range of each band is modeled. In particular the exponential wide band model was coded. Band strengths and widths are related to parameters obtained from statistical mechanics. The correlation parameters used for H_2O and CO_2 (Refs. 1 and 2) are shown in Table 1. Five wavelengths for H_2O and six for CO_2 were deemed important for the analysis:

$$\lambda_{H2O} = 71,\ 6.3,\ 2.7,\ 1.87,\ \text{and}\ 1.38\ \mu m$$
$$\lambda_{CO2} = 15,\ 10.4,\ 9.4,\ 4.3,\ 2.7\ \text{and}\ 2.0\ \mu m$$

Narrow band models, such as those used in the JANNAF standard plume radiation code, SIRRM (Ref. 3) are the most accurate molecular radiation models currently available. However, the spectral integration required to use such models is too computationally intensive for use in a coupled solution. A comparison of total radiation for the SSME was made for the mean, wide, and narrow band (from SIRRM computations) models, and is shown in Table 2. A line-of-sight calculation was used to determine the SIRRM results. The emissivity computed from the mean band model is clearly inferior to the other two spectral methods. Differences between the wide and narrow band models are evident at the higher pressures, but the experimental molecular band model data in SIRRM were not collected at these high pressures. Since some of the wide band model data were taken at higher pressures, this method of correlation was chosen for further study. Comparison of these methods to a blackbody confirms the spectral nature of radiation throughout

Table 1

Wide band model correlation parameters for various gases

Band Location λ [μm]	(δ_k)	Pressure Parameters n	b	Correlation Parameters α_0 [$cm^{-1}/(g/m^2)$]	γ_0	ω_0 [cm^{-1}]
H_2O	$m = 3$, $\eta_1 = 3652\,cm^{-1}$, $\eta_2 = 1595\,cm^{-1}$, $\eta_3 = 3756\,cm^{-1}$, $g_k = (1, 1, 1)$					
71 μm[a]	$\eta_c = 140\,cm^{-1}$ (Rotational) (0,0,0)	1	$8.6\sqrt{\frac{T_0}{T}} + 0.5$	44,205	0.14311	69.3
6.3 μm	$\eta_c = 1600\,cm^{-1}$ (0,1,0)	1	$8.6\sqrt{\frac{T_0}{T}} + 0.5$	41.2	0.09427	56.4
2.7 μm	$\eta_c = 3760\,cm^{-1}$ (0,2,0)			0.2		
	(1,0,0) (0,0,1)	1	$8.6\sqrt{\frac{T_0}{T}} + 0.5$	2.3 23.4	0.13219[b,c]	60.0[b]
1.87 μm	$\eta_c = 5350\,cm^{-1}$ (0,1,1)	1	$8.6\sqrt{\frac{T_0}{T}} + 1.5$	3.0	0.08169	43.1
1.38 μm	$\eta_c = 7250\,cm^{-1}$ (1,0,1)	1	$8.6\sqrt{\frac{T_0}{T}} + 1.5$	2.5	0.11628	32.0
CO_2	$m = 3$, $\eta_1 = 1351\,cm^{-1}$, $\eta_2 = 666\,cm^{-1}$, $\eta_3 = 2396\,cm^{-1}$, $g_k = (1, 2, 1)$					
15 μm	$\eta_c = 667\,cm^{-1}$ (0,1,0)	0.7	1.3	19.0	0.06157	12.7
10.4 μm	$\eta_c = 960\,cm^{-1}$ (−1,0,1)	0.8	1.3	2.47×10^{-9}	0.04017	13.4
9.4 μm	$\eta_c = 1060\,cm^{-1}$ (0,−2,1)	0.8	1.3	2.48×10^{-9}	0.11888	10.1
4.3 μm	$\eta_u = 2410\,cm^{-1}$ (0,0,1)	0.8	1.3	110.0	0.24723	11.2
2.7 μm	$\eta_c = 3660\,cm^{-1}$ (1,0,1)	0.65	1.3	4.0	0.13341	23.5
2.0 μm	$\eta_c = 5200\,cm^{-1}$ (2,0,1)	0.65	1.3	0.060	0.39305	34.5

Table 2

TOTAL GAS RADIATION - cal/cm^2-s

SSME				
	Mean	Wide	Narrow	σT^4
CHAMBER P=194.4 atm T=3626.02K L=43.98 cm P_w= 134.5 atm	234	90.7	124	234
THROAT P=115 atm T=3450K L=25.42 cm P_w= 81.1 atm	192	65.8	98.4	192
EXIT P=0.1943 atm T=1279K L=230.436 cm P_w= 0.15 atm	0.692	0.621	0.63	3.62

the rocket motor. A similar comparison is made for gaseous products for the ASRM 48-5, in Table 3.

2.2 Scattering (large) Particles

Optical properties for Al_2O_3 were obtained from Grumman's OPTROCK data (Ref. 4). Plots of the refractive index N_1 and the absorptive index N_2 are given in Figs. 1 and 2. These data were transformed to radiation properties by a Mie scattering code (Ref. 5) which determines absorption and scattering cross-sections as well as phase functions. The OPTROCK data includes wavelengths ranging from 0.2 to 25 μm. Additional work has been reported (Ref. 6) to provide curve-fits of the absorptive index for the Al_2O_3 optical property data.

Scattering angle dependence on the diffractive, reflective and absorptive processes are determined through the phase function, P, as illustrated in Fig. 3. Note that a specific value of $\log_{10} P$ is computed for each scattering angle COS (Θ). These figures indicate that as the size parameter ($X = \pi D/\lambda$) increases, forward scattering increases. It is known that Mie scattering is a good approximation for forward scattering for large non-spherical particles. Since extinction is dominated by scattering in the forward direction (as seen in the figures), then scattering is not very sensitive to particle shape. This justifies using the Mie theory. Comparison of radiation properties between SIRRM and the Mie code is shown in Table 4.

A line-of-sight (LOS) code was also used to determine radiance from particles. Comparison between SECA's two-flux model (Ref. 7) and the two-flux method in SIRRM appear in Fig. 4 for SSME and ASRM nozzles. A wavelength range from 0.6 to 8.0 μm was used in the two-flux method. The results indicate

TOTAL GAS RADIATION - cal/cm^2-s

Table 3

ASRM 48-5			
	Mean	Wide	σT^4
CHAMBER P=43 atm T=3513K L=105.184 cm P_w= 5.76 atm P_c= 0.57 atm	91.1	51.4	206
THROAT P=25 atm T=3230K L=24.918 cm P_w= 3.40 atm P_c= 0.33 atm	21.6	22.1	147
EXIT P=1.04 atm T=2200 K L=67.95 cm P_w= 0.14 atm P_c= 0.014 atm	2.48	2.53	31.7

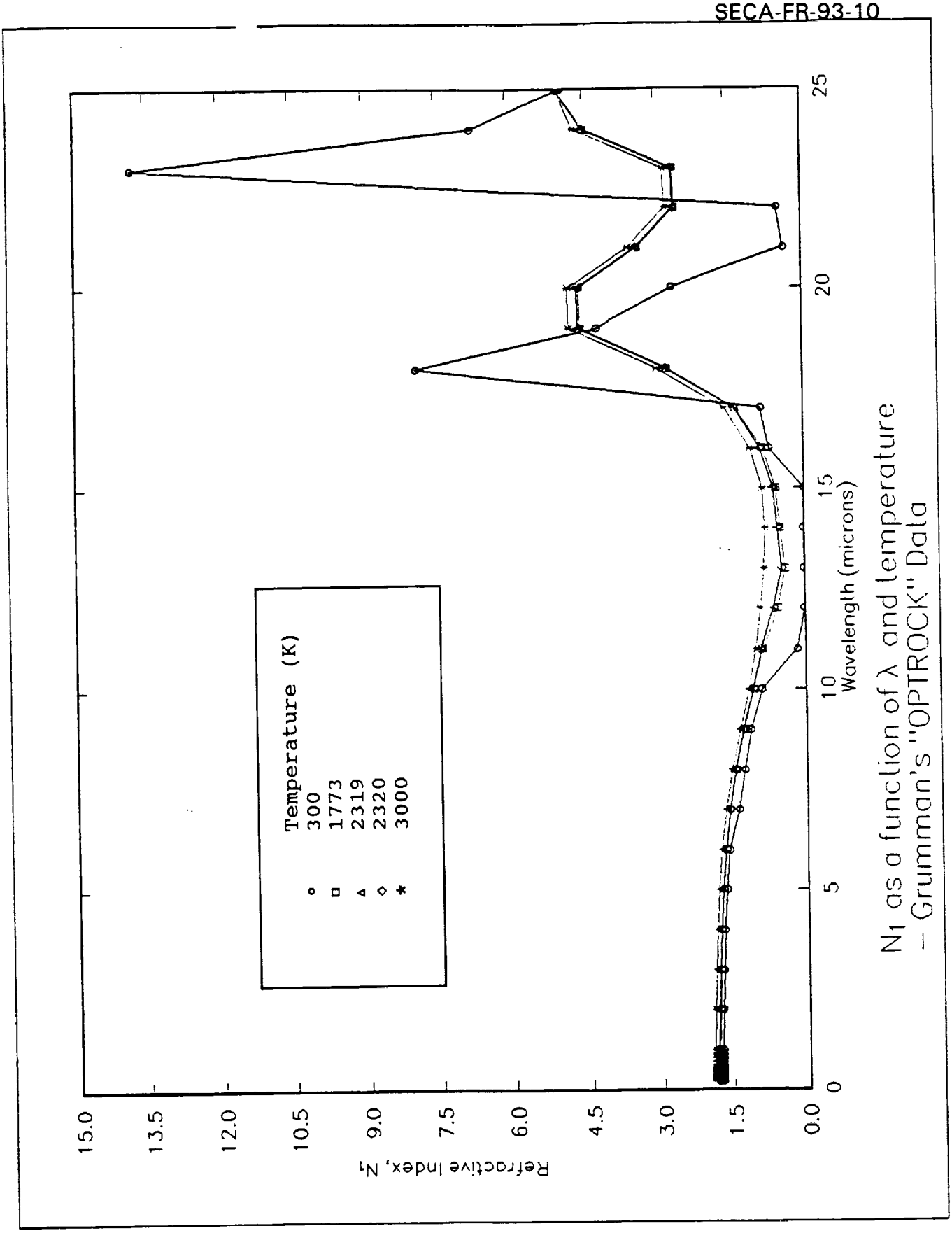
N1 as a function of λ and temperature
– Grumman's "OPTROCK" Data
Refractive Index, N1
Wavelength (microns)
Temperature (K)
300
1773
2319
2320
3000
0.0
1.5
3.0
4.5
6.0
7.5
9.0
10.5
12.0
13.5
15.0
0
5
10
15
20
25

Figure 1

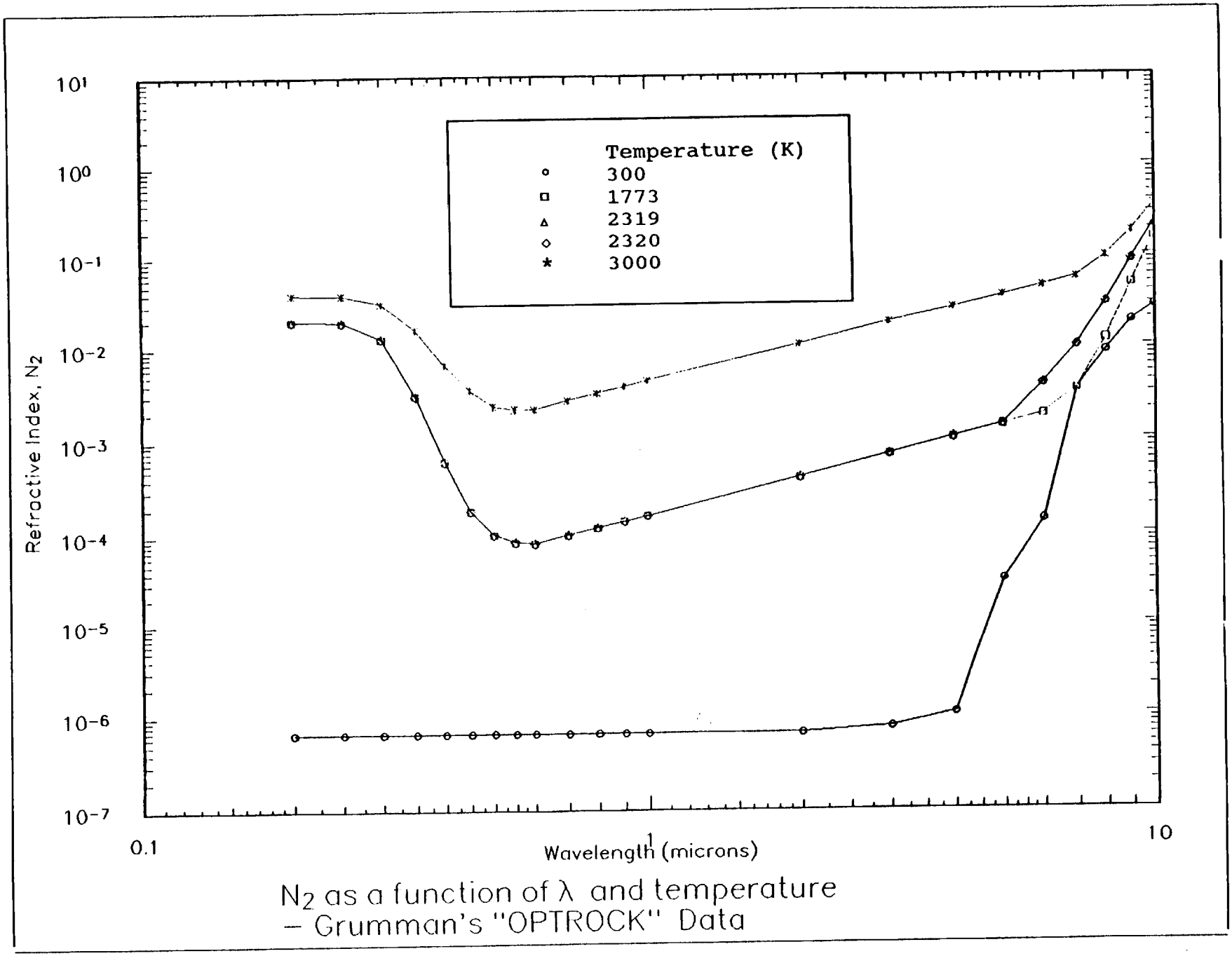
Temperature (K)
300
1773
2319
2320
3000
Refractive Index, N2
10¹
10⁰
10⁻¹
10⁻²
10⁻³
10⁻⁴
10⁻⁵
10⁻⁶
10⁻⁷
0.1
1
10
Wavelength (microns)
N2 as a function of λ and temperature
– Grumman's "OPTROCK" Data

Figure 2

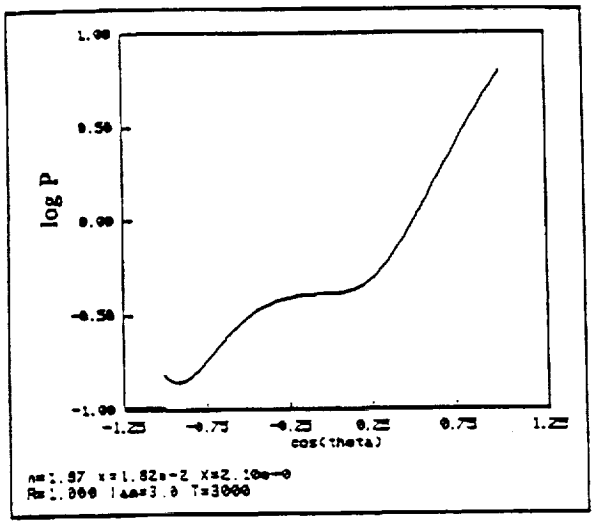

PHASE FUNCTION AS DETERMINED BY MIE THEORY CALCULATION

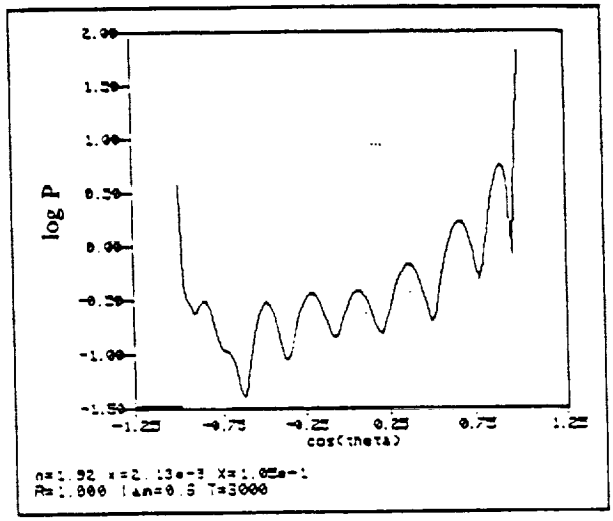

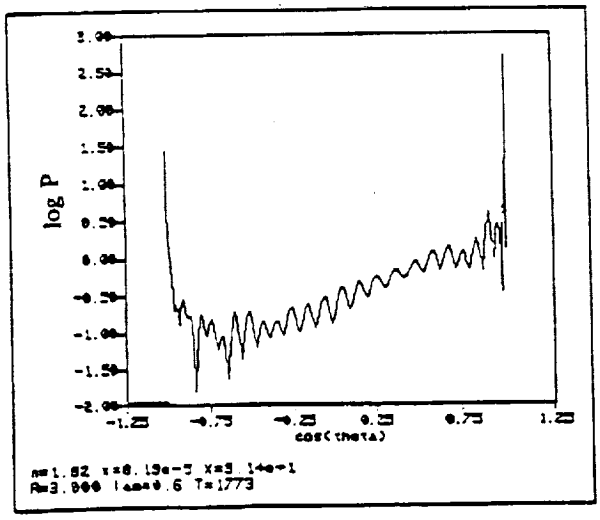

Optical properties: n,κ
Particle Radius: R
Wavelength: lam
Temperature: T
Particle Size
Parameter: $X=2\pi R/\lambda$

Figure 3

Table 4

Al_2O_3 RADIATION PROPERTIES

r, (μm)	Wave Number	σ_e, (cm^2)	Albedo	s_b	b_b	b_2	T(K)	
1.0E-3	400	6.181E-19	5.565E-10	.14352	.21295	.49999	3000	OS
		6.181E-19	5.565E-10	.1439	.2120	.5065		OM
3	5000	6.7430E-7	.98982	.073316	.061334	.087562	2320	RS
		5.956E-7	.9905	.07461	.06874	.14723		RM
3	10000	6.3054E-7	.99193	.059637	.053251	.070317	2320	RS
		6.618E-7	.9924	.05366	.05025	.10287		RM
3	3333	6.841E-7	.98754	.08270	.07050	.11115	2320	RS
		8.103E-7	.9831	.06509	.08108	.17645		RM
3	10000	6.723E-7	.98954	.07248	.060389	.085913	1773	RS
		6.752E-7	1.000	.05096	.05813	.11004		RM
3	10000	6.843E-7	.81057	.06522	.04385	.060442	3000	RS
		6.445E-7	.8666	.05318	.03896	.09529		RM

OS Original Al_2O_3 Optical Properties in SIRRM

OM Original Al_2O_3 Optical Property Data With MIE Code

RS OPTROCK Properties in SIRRM

RM OPTROCK Properties Calculated With A MIE Code

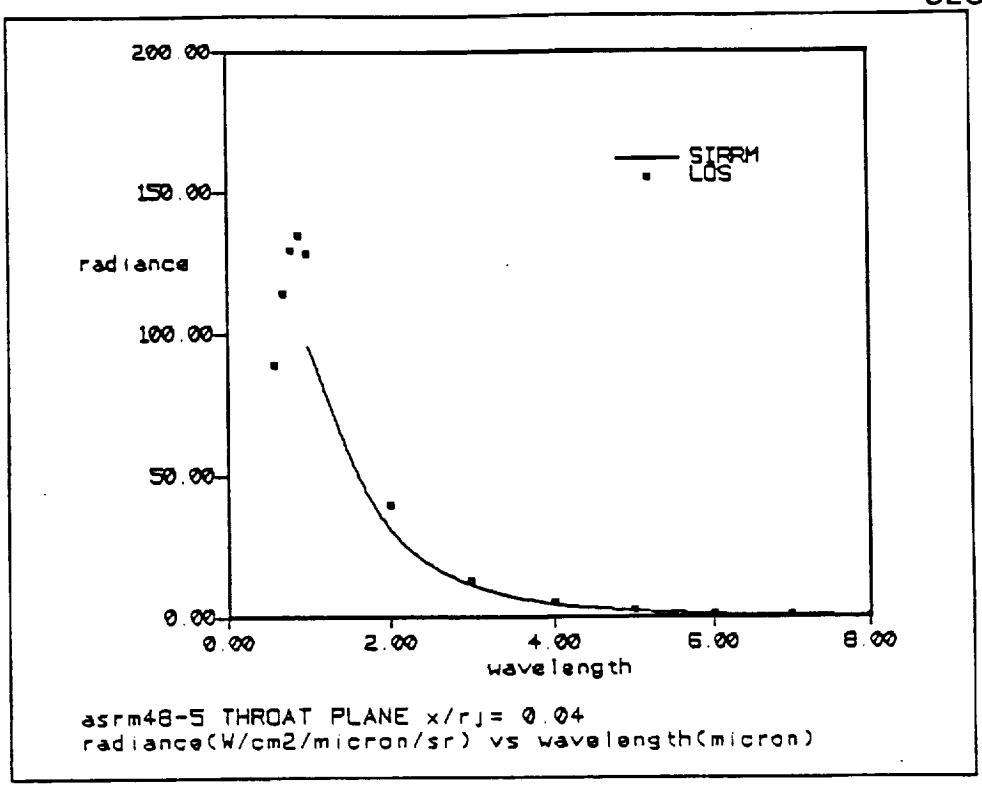
200.00
150.00
100.00
50.00
0.00
radiance
SIRRM
LOS
0.00
2.00
4.00
6.00
8.00
wavelength
asrm48-5 THROAT PLANE x/rj= 0.04
radiance(W/cm2/micron/sr) vs wavelength(micron)

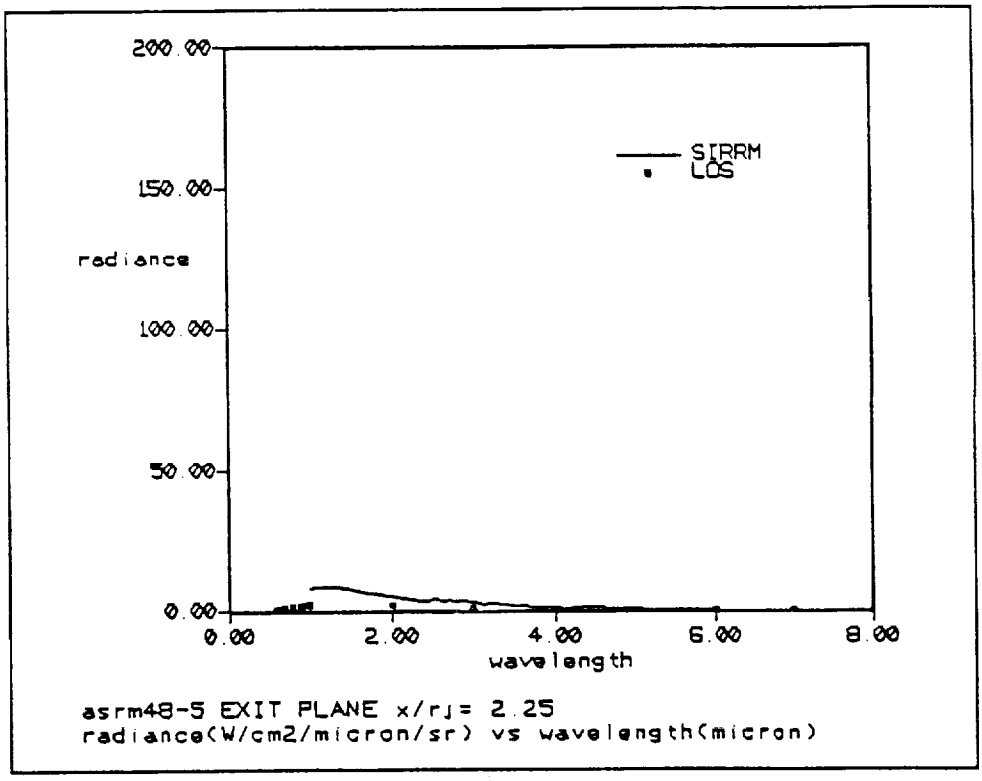
200.00
150.00
100.00
50.00
0.00
radiance
SIRRM
LOS
0.00
2.00
4.00
6.00
8.00
wavelength
asrm48-5 EXIT PLANE x/rj= 2.25
radiance(W/cm2/micron/sr) vs wavelength(micron)

Figure 4

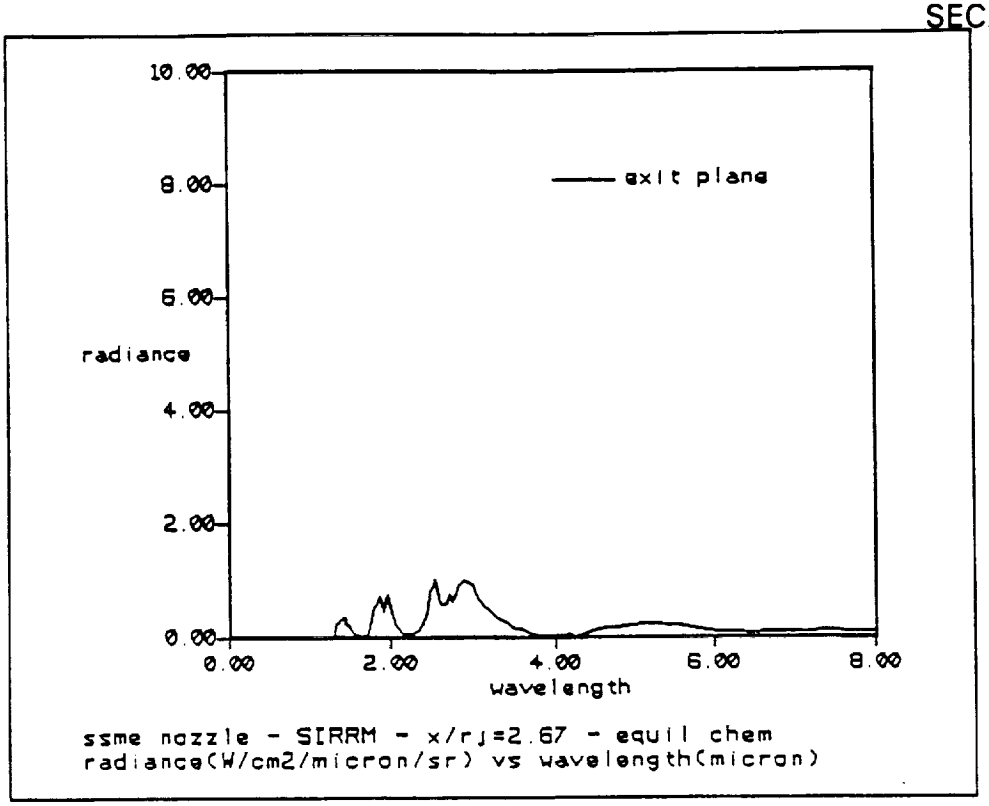

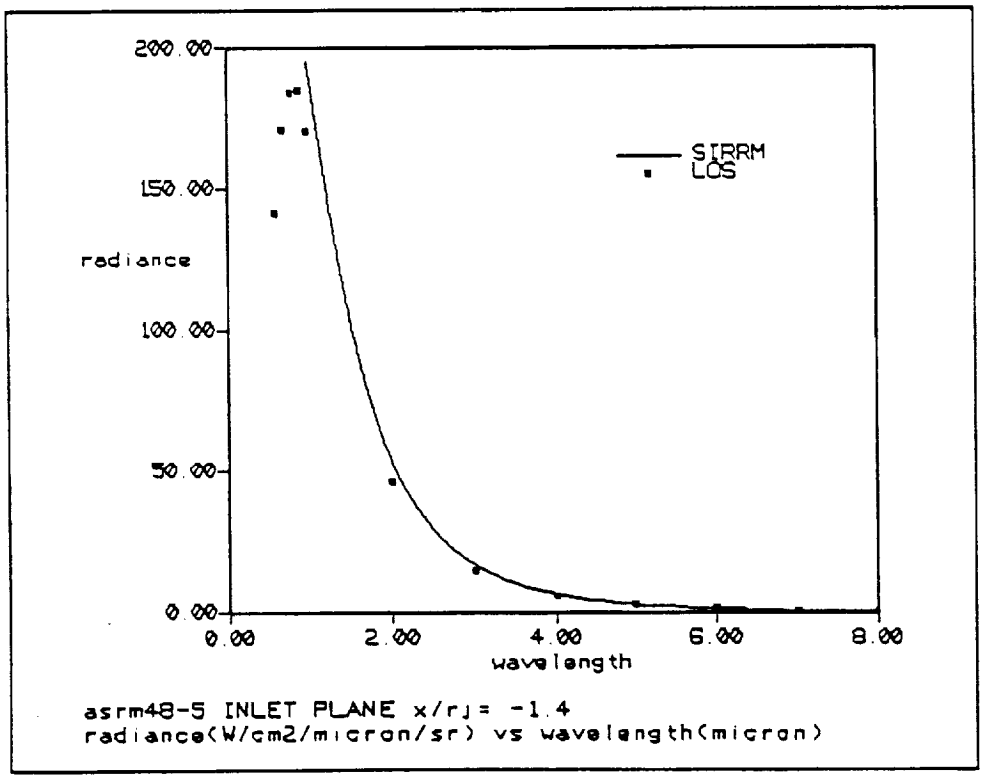

Figure 4 (Cont.)

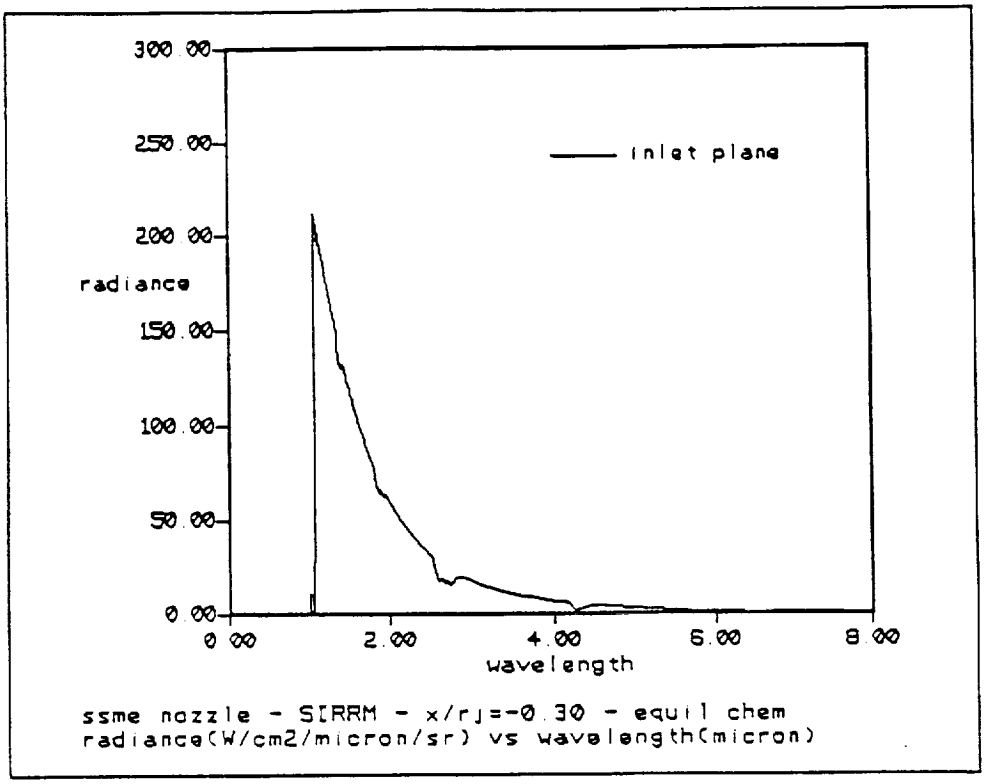

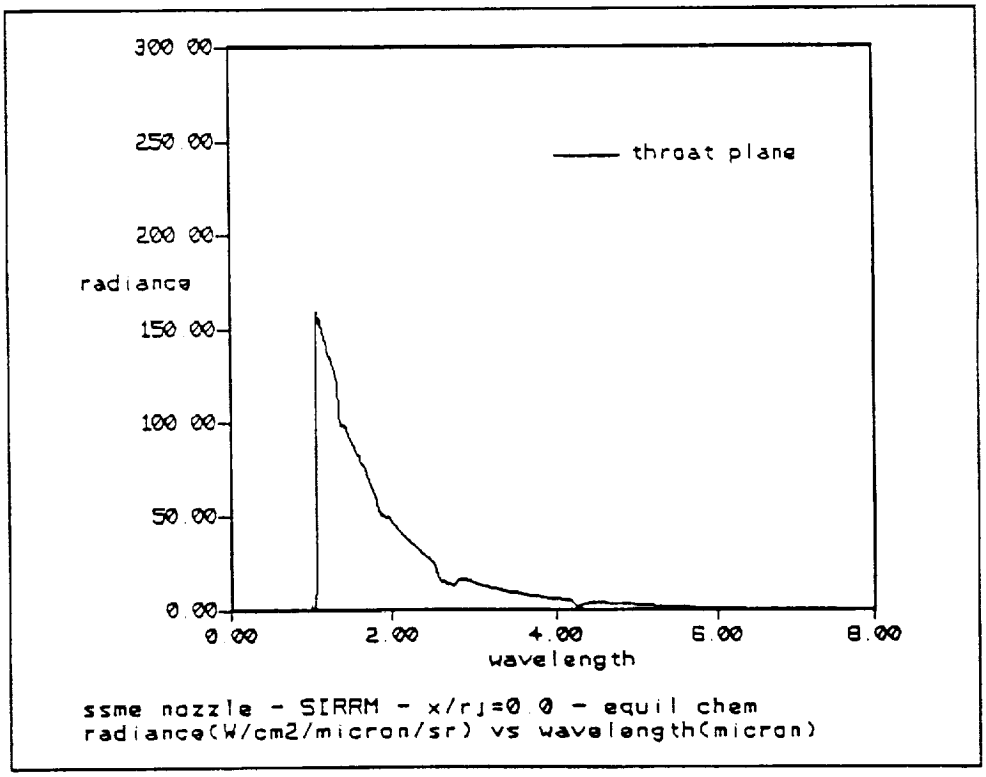

Figure 4 (Cont.)

that SECA's two-flux method is essentially identical to that in SIRRM. Although the two-flux method could be used for the present coupling analysis, many LOS calculations would be required to evaluate the volume-averaged intensity at each grid point. To reduce the computations required, the differential approximation to the RTE was chosen.

3.0 Radiative Transport Equation

The nature of the radiation/convection coupled problem is that the divergence of the radiative heat flux, $\vec{q}_r$, must be included in the energy equation and that the local spectral intensity, I_λ, of the radiation must be determined by a solution to the RTE (Ref. 8). The divergence of the radiative flux is given by:

$$\nabla\cdot\vec{q}_r = \int_0^\infty \kappa_\lambda \left[4\ \pi\ I_{\lambda b}(T) - \int_{4\pi} I_\lambda(\vec{r},\vec{\Omega})\, d\vec{\Omega}'\right] d\lambda \qquad (1)$$

The RTE is given by:

$$\vec{\Omega}\cdot\nabla I_\lambda(\vec{r},\vec{\Omega}) = \kappa_\lambda I_{\lambda b}(T) - (\kappa_\lambda + \sigma_\lambda) I_\lambda(\vec{r},\vec{\Omega}) + \frac{\sigma_\lambda}{4\pi}\int_{4\pi} P(\vec{r},\vec{\Omega}'-\vec{\Omega})\, I_\lambda(\vec{r},\vec{\Omega}')\, d\Omega' \qquad (2)$$

where κ and σ are the absorption and scattering coefficients, respectively, $I_{\lambda b}$ is the Planck blackbody function, λ is the wavelength, and $\vec{r}$ and $\vec{\Omega}$ indicate position and direction, respectively, integrated over 4 π solid angles $d\Omega'$. The I_λ is determined by solving Eq. 2 along several lines-of-sight for each point in the flowfield for each wavelength, or by using a further approximation.

4.0 Approximations to the RTE

4.1 Ordinary Differential Approximation (ODA)

The radiative intensity appears within the scattering integral of Eq. 2, resulting in an integro-differential equation. This results in a very costly system to solve. Consequently, the RTE was transformed to a simpler equation via a differential approximation. In this method the integral terms in Eq. 1 and Eq. 2 are evaluated by using the method of moments or spherical harmonics. Both the phase function and radiative intensity are rewritten as a generalized Fourier Series using Legendre Polynomials, with N terms in the spherical-harmonics expansion (the P_N - approximation). The ordinary differential approximation (ODA) (Ref. 2, 9 and 10), also known as the P_1 - approximation, involves the solution to a partial differential equation to evaluate the integrated form of the RTE. Only the terms up to first order are retained in the series, resulting in:

$$P(\vec{r}, \vec{\Omega}' - \vec{\Omega}) = 1 + \rho_1 \vec{r} \cdot (\vec{\Omega}' - \vec{\Omega}) \tag{3}$$

$$\nabla \cdot \left(\frac{1}{1 - \rho_1 \omega / 3} \nabla G \right) = - \Lambda^2 (4\pi I_b - G)_\lambda \tag{4}$$

$$\vec{q}_r = \frac{1}{3\gamma_1 \sigma_{ext}} \nabla G \tag{5}$$

where

$$\Lambda^2 = 3 \gamma_o \gamma_1 \sigma_{ext}^2$$

$$\gamma_o = 1 - \omega \rho_o$$

$$\gamma_1 = 1 - \omega \rho_1 / 3$$

σ_{ext} is the extinction coefficient (absorption + scattering), ω is the albedo defined as the scattering coefficient divided by the extinction coefficient, ρ_0 and ρ_1 are the zero and first order scattering phase function parameters used in the expansion, respectively, and G is the incident radiation at a point

$$G(r) = \int_{4\pi} I(\vec{r},\vec{\Omega}')d\vec{\Omega}' \tag{6}$$

For $\rho_0 = 1$ and $\rho_1 = 0$ the phase function defines linear isotropic scattering, while for ρ_0 and ρ_1 different from zero, linear anisotropic scattering is represented. Only linear isotropic scattering is coded at this time.

A loss of generality results in that only optically thick media can be accurately described by the P_1 - approximation. Since the combustor region of a rocket motor is optically thick, the P_1 approximation was applied to that region. Writing Eq. 4 in cylindrical coordinates results in

$$\frac{1}{r}\frac{\partial}{\partial r}\left(r\frac{\partial G}{\partial r}\right) + \frac{1}{r^2}\frac{\partial^2 G}{\partial \phi^2} + \frac{\partial^2 G}{\partial r^2} - \Lambda^2 G = -4\pi\Lambda^2 I_b(T) \tag{7}$$

For the axisymmetric nozzle, the azimuthal term (ϕ) drops out. Although Eqs. 6 and 7 are a function of wavelength, the λ was removed for brevity.

The P_1 - approximation eliminates the need to resolve the complicated angle dependencies within the integral of Eq. 6. Along with Eq. 7, Marshak's boundary conditions were used:

$$\frac{\partial G}{\partial r} = 0 \qquad (Symmetry\ axis\ at\ r = r_1)$$

$$\frac{\partial G}{\partial r} + hG = 4\pi h I_b \qquad (wall\ at\ r = r_2)$$

$$\frac{\partial G}{\partial z} \pm hG = \pm 4\pi h I_b \qquad inlet:\ Z=Z_1(-) \quad exit:\ Z=Z_2(+) \tag{8}$$

$$h = 1.5\ \sigma_{ext}\ \gamma_1 \left(\frac{\epsilon}{2-\epsilon}\right)$$

For cases in which the boundary does not radiate back into the interior, the right-hand-side of the second and third lines in Eq. 8 become zero. Presently, the code sets the boundary emissivity ϵ to 1 and the right-hand-side of Eq. 8 to 0 to represent complete absorption by the wall. However, provisions have been made to allow the boundaries to radiate back into the interior by setting a switch in the code, when $\epsilon = 1$, such that the RHS of Eq. 8 is evaluated.

4.1.1 Radiation Coupling to FDNS

The radiation source term was added to FDNS and calculated at every n global iterations, where n was chosen by computational experiments so as to reduce the computational expense of frequent coupling. Within each call to the radiation module, the current values of temperature, pressure and species number density obtained from the flow solution were used to generate new radiation properties (σ_{ext}, ω, G) and then radiation intensity at each point. It is easier to solve for the radiation source term within physical space coordinates, after which it

can be re-cast in computational space coordinates quite simply. Also, radiation grid densities different from flowfield grid densities could be used by following this procedure. Following the procedure that transformed the energy equation from physical to computational space, and normalizing with reference values, the radiative source term is added to the right-hand side of the energy equation in FDNS as

$$-\nabla \cdot \vec{q}_r = \frac{J^{-1}}{Boltzmann\ Number} \kappa \sum_{\lambda} (4 \pi I_b - G) \Delta \lambda \qquad (9)$$

where

$$Boltzmann\ number = \frac{(\rho u C_p T)_{ref}}{\sigma T_{ref}^4}$$

J is the transformation Jacobian, and σ is the Stefan-Boltzmann constant. The Boltzmann number is the ratio of radiative to convective heating. No other terms need to be added to the Navier-Stokes equations since the following effects are negligible: radiation pressure, spectral doppler shift (due to material motion), and change in material thermal energy (due to material coupling). The source term is added to the interior grid points only; no special treatment is required for the heating rate boundary condition, as the gradients imposed at the wall points will adjust to the interior values. The subroutines that were developed for the ODA procedure are discussed in the Appendix.

4.1.2 Gaseous Radiation Example

Equations 7 to 9 were discretized and added to the FDNS code. A test case was run using a Rocketdyne motor which burned RP-1 and O_2. Once a converged solution was obtained without radiation, the radiation computations were initiated. No soot particles were considered in this case. The values of G were initialized with Planck functions at eleven wavelengths (H_2O and CO_2) at each flowfield grid

temperature. Eleven equations of the form of Eq. 7 were solved using an SOR method, with convergence occurring within 10 iterations. Once the value of G was computed at each interior point, the boundary values were determined according to Eq. 8 with boundary emissivity set to 1 and with no boundary re-radiation. The radiation computations were called every 50 iterations with a 0.1 percent change in the source term from the previous call.

Subsequently, the radiative source terms were evaluated and added to the energy equation. However, the solution did not show any appreciable difference in the temperature field due to the radiation source terms in either case. For the coupling radiation/convection nozzle flow solution, two limits were observed. In the high limit, the magnitude of the radiation source term was as large as ten times the non-radiative source term within the combustor, and in the low limit, as low as 0.01 times the non-radiative source term (near the wall). In either situation, radiation still has a negligible effect on the flowfield. This may seem contradictory at first. However, this behavior follows from the way in which FDNS evaluates the source terms. The explicit or right-hand-side source terms include dissipation, conduction, the off-diagonal convection terms, wall function terms next to the wall, plus the radiation term. Diagonal convection terms are split off from the right-hand-side and moved to the left-hand-side to become implicit source terms. Since the implicit source terms in the energy equation dominate the explicit radiation term by a factor of 1e4 in the low limit, it is clear that the radiation source term is negligible compared to the other source terms. For cases where the implicit source term is zero, as in the high limit, the total explicit source term was negligible with or without radiation.

The negligible radiation in the combustor is due to two effects: a constant temperature field and the large Boltzmann number of 7700. To test conditions for

which radiation could be important, a hypothetical test case was constructed: a linear variation in temperature was imposed across the motor, and the Boltzmann number was multiplied by a factor of 1e-4. Temperature contours of this start solution are presented in Fig. 5. After 2000 iterations of radiation coupling, the temperature contours take the form shown in Fig. 6. Comparison of radiation and non-radiation temperature contours indicates a reduction of temperature in the combustor and an increase of temperature in the nozzle with an average of five percent in each case, and that the source term was opposite in sign to that in the combustor due to the cold flow there. This test indicates that radiation can be expected to be important for cases where the temperature field differs from point to point, and where the convective heating rate does not completely dominate the radiation component. It can be concluded that radiation in the optically thick combustor region of the Rocketdyne test case was minimal at best.

4.1.3 Particulate Radiation Example

A coupled particulate radiation/CFD solution has not yet been attempted. All of the necessary Al_2O_3 radiation subroutines have been added to FDNS, and computations can be made in the future to evaluate the effects of particles on flowfield properties.

4.2 Improved Differential Approximation (IDA)

The IDA was developed to extend the validity of the P_1 - approximation to also predict optically intermediate conditions. It involves a two-step process: the first is to obtain G from the P_1 - approximation, the second is to upgrade this solution by substitution into an additional partial differential equation (Ref. 2 and 11). There is no integro-differential equation to solve; however, an evaluation of

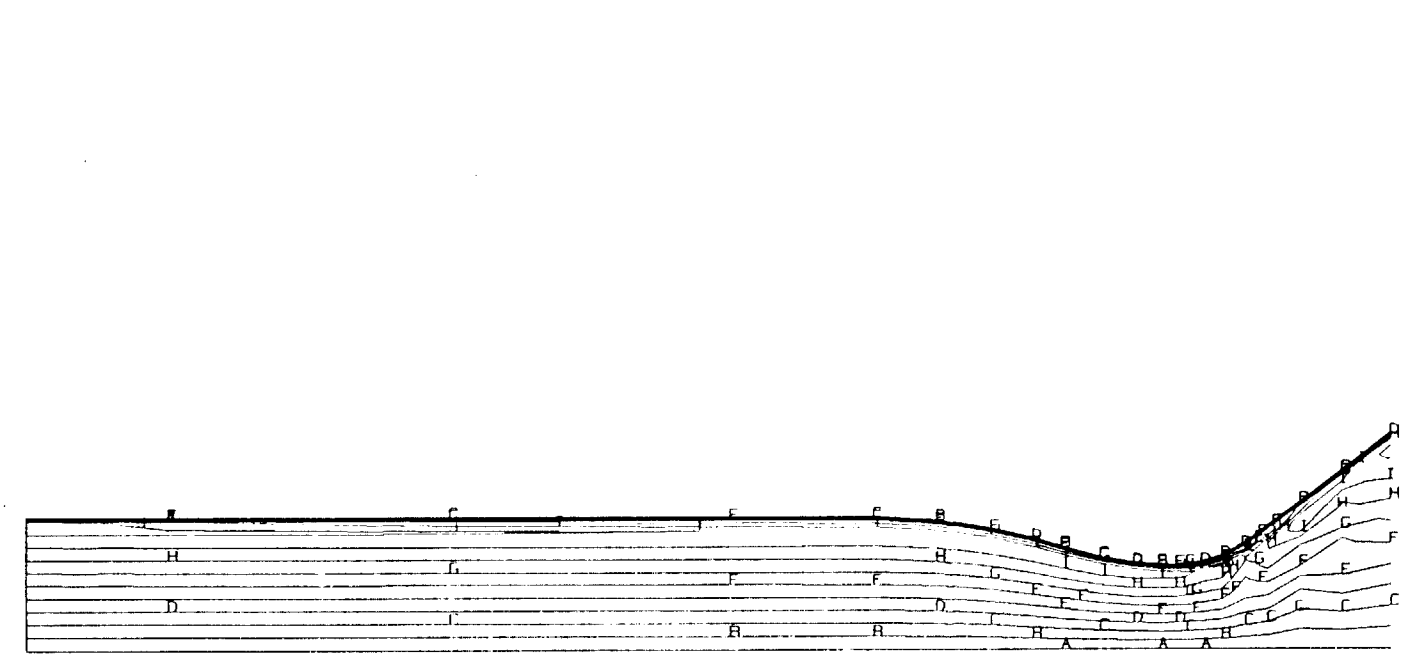

TEMPERATURE

Figure 5

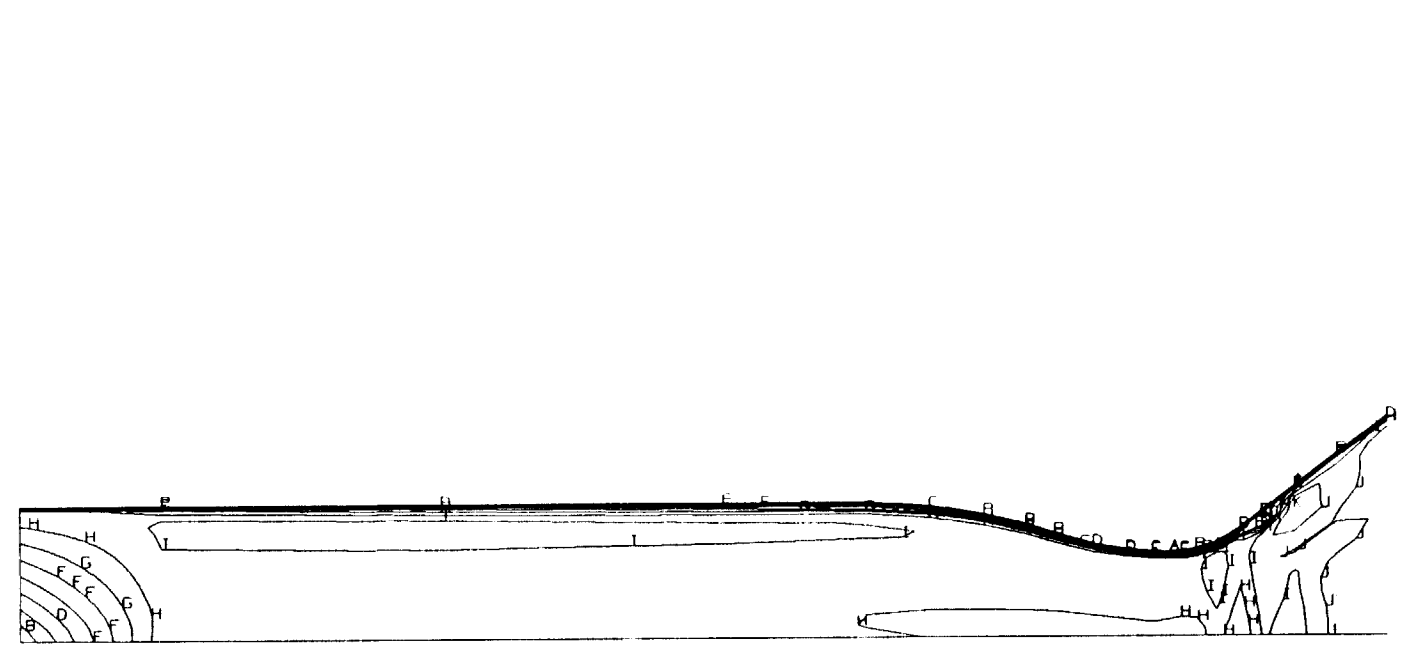

TEMPERATURE

Figure 6

several integrals is required. The following development will delineate the three steps required to obtain an IDA solution: i.) solution to ODA, ii.) solution to a surface integral equation for wall radiosities, and iii.) evaluation of surface integrals for points inside the medium. The source term to the ODA can be written

$$S^*(\vec{r},\vec{\Omega}) = (1-\omega)\, I_b^*(\vec{r}) + \frac{\omega}{4\pi}\left[G^*(\vec{r}) + \rho_1\, \vec{q}(\vec{r})\cdot\vec{\Omega}\right] \tag{10}$$

Equation 10 was obtained from Eq. 4 after transforming the independent variables (r, z) to (γ_r, γ_z). Also, the asterisk in Eq. 10 denotes the ODA or intermediate solution.

A solution for I_λ can be constructed from terms related to wall (w) and medium (m) contributions.

$$I(\vec{r},\vec{\Omega}) = I_m(\vec{r},\vec{\Omega}) + I_w(\vec{r},\vec{\Omega}) \tag{11}$$

where

$$I_m(\vec{r},\vec{\Omega}) = \int_0^{\tau} S^*(\vec{r}' + \Omega'\vec{\Omega}, \vec{\Omega})\, e^{-(\tau_s - \tau_s')}\, d\tau_s' \tag{12}$$

and

$$I_w(\vec{r},\vec{\Omega}') = \frac{J_w(\vec{r}_w)}{\pi}\, e^{-\tau_s} \tag{13}$$

It is important to note that I_w accounts for emission from the enclosure wall (that may have been attenuated by absorption and scattering in the medium and by reflections from the walls). I_m is a function of the radiation released within the medium into a given direction by emission and scattering, and as such is related to the radiative source term (Ref. 2).

The crux of the IDA is the way the source term is approximated. In optically thin regions, the scattering integral is negligible (the last two summations in Eq.

10) and attenuation follows a linear variation. These observations justify approximating the source term integral in Eq. 12 by a Taylor series. This results in the following representation for the medium:

$$I_m(\vec{r},\vec{\Omega}) \approx S^*(\vec{r}-\Omega_0\vec{\Omega},\vec{\Omega})\,(1-e^{-\tau_s}) \tag{14}$$

where τ_s refers to the optical distance between two points along a path length s (in this case from a point of interest in the medium to a point on the wall):

$$\tau_s = \int_0^s \sigma_{ext}\, ds \tag{15}$$

The source term in Eq. 14 is evaluated at an adjusted point corresponding to an optical distance τ_0 away from the point of interest, according to:

$$\tau_0 = 1 - \frac{\tau_s e^{-\tau_s}}{1-e^{-\tau_s}} \tag{16}$$

This form for S^* is a consequence of using the assumed linearity of S^* in reverse, i.e., by linearly varying S^* from the wall to the point under consideration.

Radiosity from a particular wall point is composed of emission plus radiance on that point from other wall points, multiplied by the appropriate attenuation factor. Specifically,

$$J_w(\vec{r}) = \epsilon\pi I_{bw}(\vec{r}) + (1-\epsilon)\int_A [J_w(\vec{r}_w)\,e^{-\tau_s} + \pi I_m(\vec{r},\vec{\Omega})]\,\frac{\cos\theta\cos\theta_w}{\pi S^2}\,dA \tag{17}$$

The integral in Eq. 17 is evaluated as a summation over each wall segment j, where the view factors must be determined. A code or subroutine like the RAVFAC code (Ref. 12) may be used for this calculation. The attenuation factors involving $e^{-\tau s}$ are then evaluated as τ_{ij} between wall points i and j. Similarly, the source term takes the form S^*_{ij} and corresponds to a value that lies between the wall points i and j according to Eq. 16.

The final step is to determine the improved value for the incident radiation G according to:

$$G(\vec{r}) = \frac{1}{\pi}\int_{4\pi}[J_w(\vec{r}_w)\,e^{-\tau_s} + \pi I_m(\vec{r},\vec{\Omega})]\,\frac{\cos\theta_w}{\pi S^2}\,dA \qquad (18)$$

The radiative source term is determined as in the ODA, using Eq. 9. Since this method is valid for all optical thicknesses, it can be used throughout the nozzle from combustor to exit, and in the plume. Most of the coding necessary to perform the IDA calculations has been made. A subroutine to implement the IDA has been written. This subroutine requires τ_s and view factors; methods to calculate these values will be developed in Phase II. A preliminary evaluation of τ_s and the required view factors was made by evaluating radiation in a cylindrical geometry configuration, as described in Section 4.3.

4.3 Radiation Heat Transfer in an Infinite Cylinder

Since view factors for an axisymmetric motor geometry were needed for implementing the IDA and since approximate methods of evaluating the optical depth between points in the motor, τ_s, are required, a cylindrical geometry was investigated. Rocket motor radiation was estimated with a diffusion approximation for a cylindrical geometry by Pearce (Ref. 13). Since LOS/view-factor analyses were to be made for a cylindrical geometry, the two-flux particle radiation model (Ref. 7) was used to provide an alternate solution to the problem Pearce posed. Such a solution involves determining the optical depth across the cylinder - data which can subsequently be used to judge how τ_s should be evaluated. The actual evaluation of τ_s will be a Phase II task. This approach also allows the development of a simple method for estimating rocket motor chamber wall radiation.

4.3.1 The LOS Method of Predicting Uncoupled Radiation

An LOS method for predicting radiation heat transfer to a point on an infinite cylinder was developed by considering the cylinder to have constant temperature and constant composition. The total hemispherical radiation heat rate to a point on the edge of a cylinder can be found from the following equation:

$$Q_{rad} = \frac{\int_0^{2\pi}\int_0^{\pi/2} q(\theta,\phi)\, d\theta\, d\phi}{\int_0^{2\pi}\int_0^{\pi/2} \cos\theta \sin\theta\, d\theta\, d\phi} \qquad (19)$$

which can be reduced for the infinite cylinder to :

$$Q_{rad} = \frac{\int_0^{\pi}\int_0^{\pi/2} q(\theta,\phi)\, d\theta\, d\phi}{2\pi} \qquad (20)$$

The term, $q(\theta,\phi)$, is the radiation heat flux to the point from a particular line of sight. It is evaluated in this line of sight code with a one-dimensional slab model using absorption and scattering OPTROCK data. Since the conditions inside the cylinder are considered isothermal and homogeneous, the radiation heat flux term for each different line of sight changes only with path length. Path lengths for a line-of-sight inside an infinite cylinder are calculated as illustrated in Fig. 7, where P_i represents the path length for a individual line-of-sight. The heat rate terms for each different path length are numerically integrated according to Eq. 20 to obtain the total hemispherical radiation heat flux to the point.

For Al_2O_3, particle radiation inputs into the program are the number and size of the particles, the particle density in the flow volume for each particle size, and temperature of each particle size.

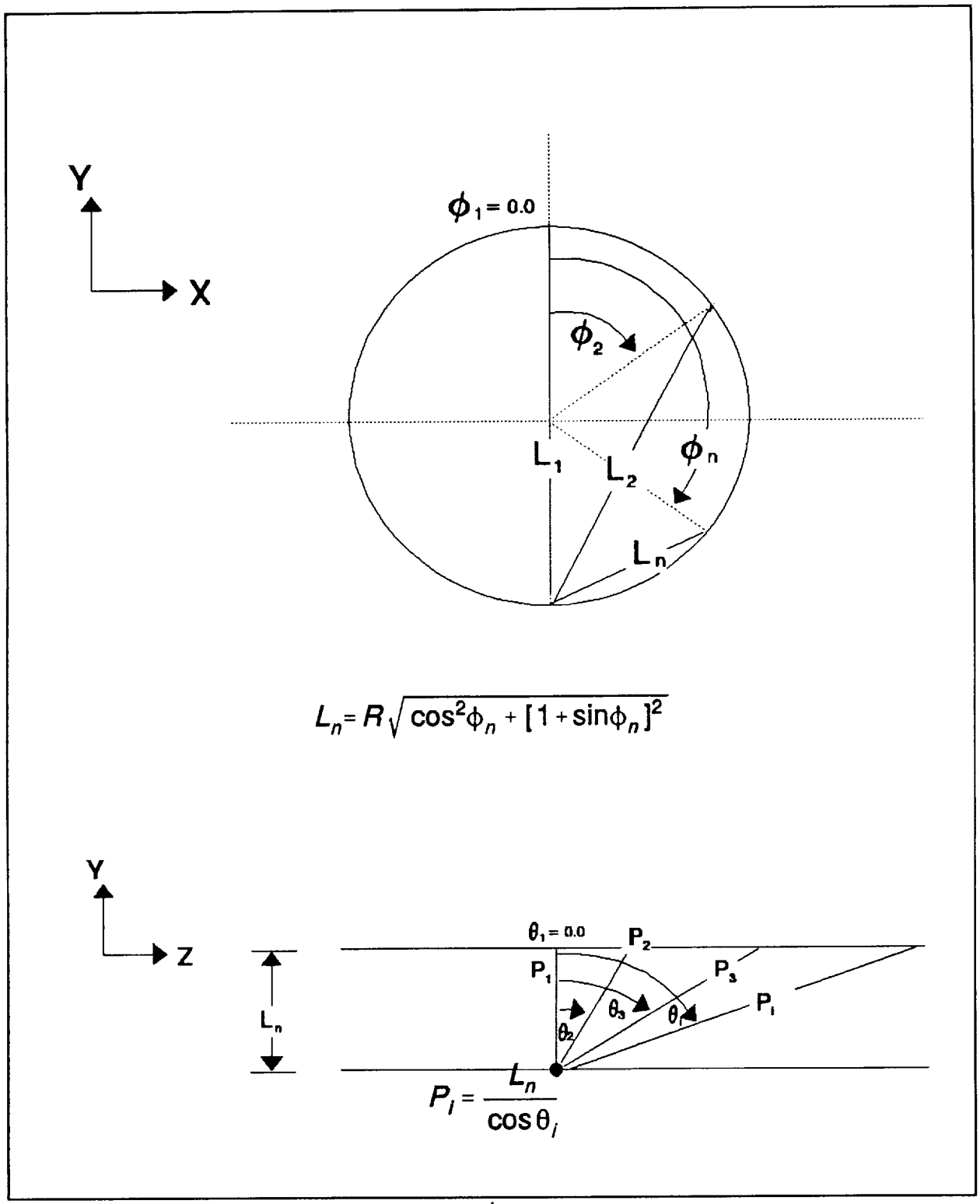

Figure 7. Path Length Calculation

4.3.2 Validation of the LOS Method

To validate the program, a case was run to compare with Pearce (Ref. 13). The inputs which were used for this comparison are shown in Table 5. Particle sizes were chosen according to the particle size distribution used by Pearce. Particle densities were calculated by multiplying particle mass flow (calculated through the number density of each chosen particle size) by the density of the flow and dividing by the total mass flow. The total mass flow and density were calculated by running the CEC program for a rocket motor of similar propellant and chamber pressure. Table 6 lists the results of both methods for a cylinder with a radius of 3 inches. These results are in good agreement. Pearce also ran a series of cases with varying nozzle throat diameters assuming the same particle distributions. This data were compared to an empirical equation for determining emissivity in a solid rocket motor. The line-of-sight method, Pearce method and the empirical method results are all compared if Figure 8. The modest differences between the Pearce method and the line-of-sight method may be due to the particle size distribution differences, CEC rocket motor predictions differences, and different particle property data for the prediction of the absorption and scattering coefficients.

Both the line-of-sight method and the Pearce method use the same assumptions of constant temperature and constant composition within the motor. Radiation predictions should be relatively accurate in the nozzle throat and combustion chamber where the assumed flow is accurate, as compared to the exit plane where temperature and density (composition) variations are more prominent.

For supersonic portions of the nozzle, other methods which account for temperature and composition variations, as well as, geometrical considerations are

warranted. The LOS method is not restricted to constant flow properties or optically dense media. If a CFD grid and properties at the grid points are provided, an uncoupled LOS calculation through the temperature and composition gradients to the nozzle walls can be made.

Table 5

Input to Program for Comparison to Pearce [13]

Particle No.	Particle Size (μm)	Particle Mass/Flow Volume (slug/ft^3) × (10^4)	Temperature (°R)
1	0.3	2.8796	5580.
2	0.5	4.3929	5580.
3	0.7	4.7292	5580.
4	1.0	3.9305	5580.
5	1.2	3.0898	5580.
6	1.5	1.9758	5580.

Table 6

Comparison of Predicted Radiation Heat Transfer @ R = 3 inches

(BTU/ft^2-s)

Pearce [13]	Line of Sight Program
66.5	70.7

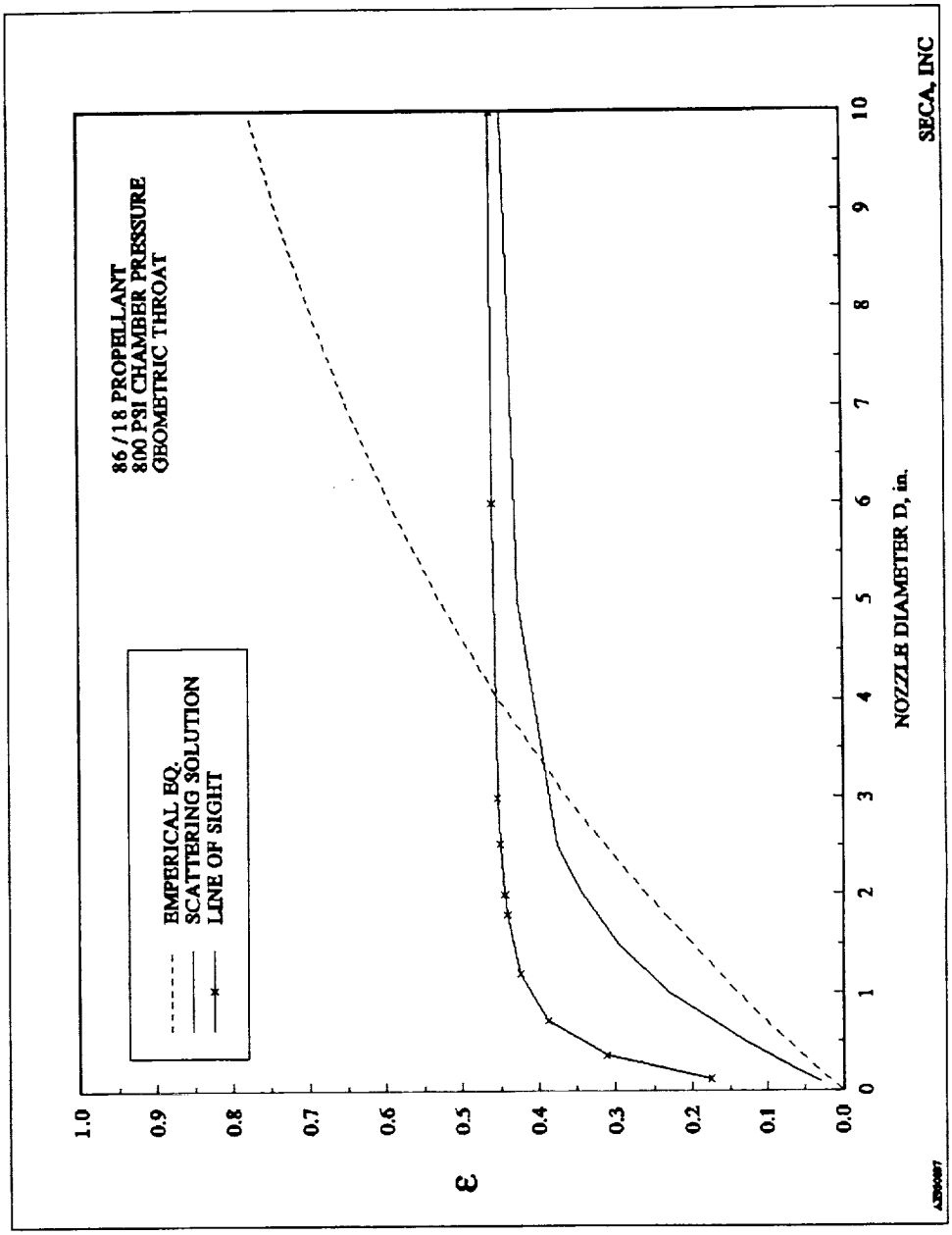

Figure 8 Comparison of Radiation Heat Tranfer Methods

5.0 Technical Feasibility

This Phase I study established that a coupled radiation/convection CFD solution for rocket motor and plume analysis is feasible using variations of the differential approximation to describe the radiative transfer. The order and type of improvement required in the differential approximation depends on the specific application. Additional data storage is required to analyze radiation/convection coupled flowfields, but the additional iterations required to reach a solution with the modified FDNS code is modest. Further Phase II research is required to obtain the generality needed to analyze all types of propellant systems of interest and to provide a sufficient number of coupled solutions to determine when this methodology is preferable to conventional uncoupled methods. Specific conclusions drawn from the Phase I study are given by the following.

The RTE was approximated by the P_1 - approximation method for application to optically thick media. A coupled radiation/convection solution was generated for an H_2/O_2 rocket using the P_1 - approximation to solve for the incident radiation at a point. This solution was driven by the extinction coefficients derived from a wide band model. Results indicate a negligible radiation effect in the combustor where the ODA is valid, for the one motor case considered, due to the very large convective effect indicated in the Boltzmann number. A hypothetical test case was run which indicated that the coupling calculation behaved properly. Particle radiation/flowfield coupling routines were completely coded, and additional runs will be made as part of a Phase II investigation.

Extension of the ODA to the IDA was begun and is almost completed. The ODA solution is the first step in obtaining an IDA solution, which is valid throughout all optical thicknesses. In particular, the IDA will be used in the nozzle

region and in the combustor to compare the differences in the two approximations. Results are not anticipated to change in the optically thick combustor, but the nozzle section should show a different solution behavior. The IDA must be used for radiation/convection coupled plume analyses.

The two-flux LOS method which was originally written for a one-dimensional plane-parallel slab geometry, was extended to cylindrical configurations. Optical thickness was computed for various angles across a single cylindrical slab. Good comparisons for radiation heating predictions were obtained between LOS and a diffusion approximation for the nozzle throat region. For optically thin regions, more slabs are required but the LOS method is still applicable. Furthermore, the LOS method can be used to advance and evaluate the development of the IDA method.

Finally, the radiation updates made to the FDNS code to provide the radiation/convection coupled solution are presented as modules on a floppy disk delivered to the technical monitor of this work. A description of the radiation module updates to FDNS is given in the appendix.

Appendix

A brief description of the radiation updates added to FDNS is given in this section. This code will be provided on a floppy disk supplied to the technical monitor of this work along with the final report.

Five of the original FDNS subroutines were upgraded to include radiation call statements and include files. Their names were appended with _RAD to signify these changes.

DATAIO_RAD:	include fdns20 include dataio3.inc include dataio4.inc
FDNS_RAD:	include fdns20 include fdns3.inc include fdns4.inc call rad0
PSOURC_RAD:	include fdns20 eliminates radiation emission term of original module since its effect is added through the radiation source term in radin0.
SOURCE_RAD:	include fdns20 include source.inc
INIT_RAD:	include fdns20 include init6.inc reads in radiation switch IRAD

New Radiation Modules

Fortran Files

astar dimensionless band absorption for H_2O and CO_2

Fortran Files (Cont.)

ecoefg	extinction coefficient for H_2O and CO_2
ecoefp	extinction coefficient for Al_2O_3
extinc	driver for extinction coefficients
htrad	radial and axial heating rate at a point (Btu/ft^2-s)
linint	double linear interpolation of particle size and temperature for the absorption coefficient
logint	double log (base 10) interpolation of particle size and temperature for the scattering coefficient
pathl	path length at each grid location
plankf	Planck function evaluation
ptlrad	transforms FDNS particle flowfield results to particle temperature and number density
rad0	driver for radiation module
radbc	radiation boundary conditions
radin0	driver for P_1 - approximation; computes radiation source term
radpl	SOR routine for incident radiation G
refrac	reads in particle refractive index (used in evaluation of Planck function) from KOCH2.PRN data
lininr	linear interpolation of refractive index as function of temperature
refrin	driver for refractive index interpolation
sigacl	particle absorption coefficients from OPTROCK data located in SIGACL.DAT
sigav	particle absorption and scattering coefficients

Fortran Files (Cont.)

sigscl	particle scattering coefficients from OPTROCK data located in SIGSCL.DAT
summa1 and summa2	wide band model summation - function of vibrational quantum number
trdiag	tridiagonal solver for P_1- approximation
widebm	wide band model for H_2O and CO_2

Data Files

BLKDAT.F	radiation data for H_2O and CO_2
KOCH2.PRN	optical property data from Grumman OPTROCK test for Al_2O_3
SIGACL.DAT	absorption coefficients for Al_2O_3 obtained from transforming KOCH2.PRN by Mie code
SIGSCL.DAT	scattering coefficients for Al_2O_3 obtained from transforming KOCH2.PRN by Mie code

Include Files

fdns20
fdns21
fdns22

alumox.inc
h2o.inc
co2.inc
source.inc
dataio3.inc
dataio4.inc
init6.inc
fdns3.inc
fdns4.inc

Initialization Modules

Fortran File

grid — initializes grid and flowfield for nozzle flow without radiation

Include Files

grid1.inc
grid2.inc — initializes normalized incident radiation per wavelength and the refractive index; writes to units 15 and 16 respectively

grid3.inc — refractive index read and interpolation modules

no provision has been made to read in separate flowfield and radiation grid files

Figure 9 presents a flow chart of the radiation driver, subroutine rad0.f.

Radiation Module Flow Chart

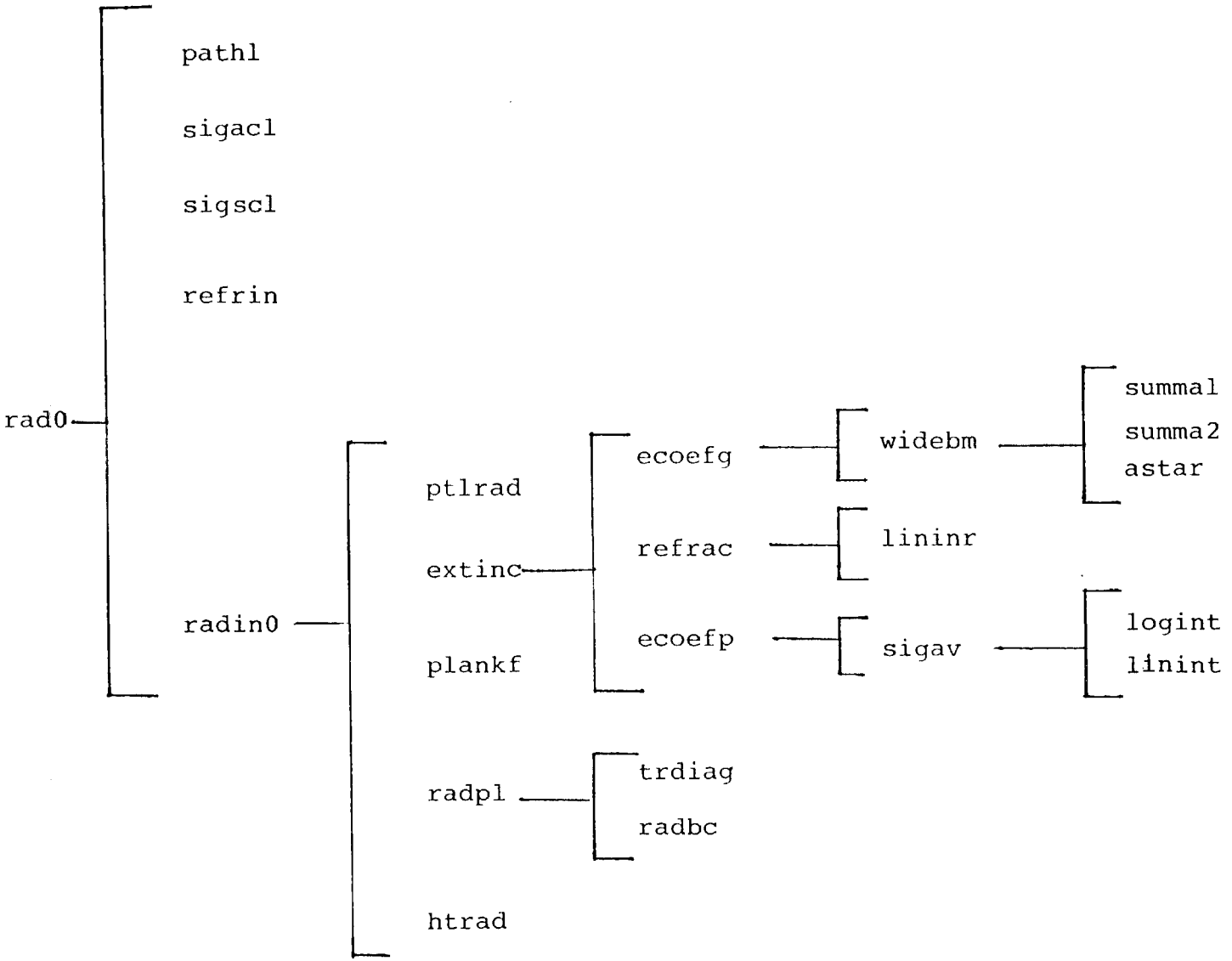

Figure 9

REFERENCES

1. Edwards, D.K., "Molecular Gas Band Radiation," in Advances in Heat Transfer, pp. 115-192, Academic Press, 1976.

2. Modest, M.F., Radiative Heat Transfer, McGraw-Hill, 1993.

3. Markarian, P., and R. Kosson, "Standardized Infrared Radiation Model (SIRRM-II)," AFAL-87-098, Grumman Aerospace Corp., Bethpage, NY, March 1988.

4. Calia, V.S., Grumman Aerospace Corp., Bethpage, NY, personal communication, August 1991.

5. Bohren, C.F. and Huffman, D.R., Absorption and Scattering of Light by Small Particles, Wiley and Long, 1983.

6. Reed, R.A., et al, "Solid-Propellant Rocket Motor Exhaust Plume Measurements and Analysis," JANNAF Plume Technology Conference, Huntsville, AL, May 1991.

7. Smith, S.D., et al, "Model Development For Exhaust Plume Effects on Launch Stand Design - PLIMP/LSD," Final Report, Contract NAS8-38472, SECA-93-FR-9, SECA, Inc., Huntsville, AL, June, 1993.

8. Siegel, R. and Howell, J.R., Thermal Radiation Heat Transfer, 2nd ed., McGraw-Hill, NY, 1981.

9. Ou, Szu-Cheng S. and Kuo-Nan Liou, "Generalization of the Spherical Harmonic Method to Radiative Transfer in Multi-Dimensional Space," J. Quant Spectrosc. Radiat. Transfer, 28, pp. 271-288, 1982.

10. Menguc, M.P. and Viskanta, R., "Radiative Transfer in Axisymmetric, Finite Cylindrical Enclosures," in Fundamentals of Thermal Radiation Heat Transfer, ASME, HTD, 40, Dec. 1984.

11. Modest, M.F., "The Improved Differential Approximation for Radiative Transfer in Multidimensional Media," J. of Heat Transfer, 112, pp. 819-821, August 1990.

12. Lovin, J.K. and Lubkowitz, A.W., "User's Manual for 'RAVFAC', a Radiation View Factor Digital Computer Program," Lockheed Missiles and Space Co., R-61321, November, 1969.

13. Pearce, B.E., "Radiative Heat Transfer Within a Solid-Propellant Rocket Motor," J. Spacecraft, 15, 2, pp. 125-128, March-April, 1978.

NASA

Report Documentation Page

1. Report No.	2. Government Accession No.	3. Recipient's Catalog No.

4. Title and Subtitle

RADIATION/CONVECTION COUPLING IN ROCKET MOTOR AND PLUME ANALYSIS

5. Report Date

July, 1993

6. Performing Organization Code

7. Author(s)

A. J. Saladino
R. C. Farmer

8. Performing Organization Report No.

SECA-FR-93-10

10. Work Unit No.

9. Performing Organization Name and Address

SECA, INC.
3313 Bob Wallace Avenue, Suite 202
Huntsville, AL 35805

11. Contract or Grant No.

NAS8-39811

13. Type of Report and Period Covered

Contractor - FINAL

12. Sponsoring Agency Name and Address

NASA/MSFC
Marshall Space Flight Center, AL 35812

14. Sponsoring Agency Code

15. Supplementary Notes

P. Sulyma/Technical Monitor

16. Abstract

A method for describing radiation/convection coupling to a flowfield analysis was developed for rocket motors and plumes. The three commonly used propellant systems; H_2/O_2, RP-1/O_2, and solid propellants; radiate primarily as: molecular emitters, non-scattering small particles (soot), and scattering larger particles (Al_2O_3), respectively. For the required solution, the divergence of the radiation heat flux was included in the energy equation, and the local, volume-averaged intensity was determined by a solution to the radiative transfer equation. A rigorous solution to this problem is intractable, therefore solution methods which use the ordinary and improved differential approximation were developed. This radiation model was being incorporated into the FDNS code, a Navier-Stokes flowfield solver for multiphase, turbulent combusting flows.

17. Key Words (Suggested by Author(s))	18. Distribution Statement
radiation/convection flowfield coupling	unclassified - unlimited

19. Security Classif. (of this report)	20. Security Classif. (of this page)	21. No of pages	22. Price
unclassified	unclassified	40	

NASA FORM 1626 OCT 86